https://doi.org/10.5194/egusphere-2026-2640
Preprint. Discussion started: 11 June 2026

Fast approximation of Antarctica's GIA response to future ice melt with 3-D Earth structure

Jan Swierczek-Jereczek[1,2,⋆], Erica M. Lucas[3,4,⋆], Natalya Gomez[3], Andrew J. Lloyd[5], Konstantin Latychev[6], and Jerry X. Mitrovica[7]

[1]Department Earth Physics and Astrophysics, Complutense University of Madrid, Madrid, Spain
[2]Geosciences Institute, CSIC-UCM, Madrid, Spain
[3]Department of Earth and Planetary Sciences, McGill University, Montréal, Canada
[4]Department of Earth and Planetary Sciences, University of California, Santa Cruz, Santa Cruz, CA, USA
[5]Lamont Doherty Earth Observatory, Columbia University, Palisades, New York, USA
[6]Seakon, Toronto, Ontario, Canada
[7]Department of Earth and Planetary Sciences, Harvard University, Cambridge, Massachusetts, USA
⋆These authors contributed equally to this work.

Correspondence: Jan Swierczek-Jereczek (janswier@ucm.es) and Erica M. Lucas (ermlucas@ucsc.edu)

Abstract. Projections of Antarctic ice mass loss and associated sea level contributions over the coming centuries are intrinsically linked to glacial isostatic adjustment (GIA), a process by which changing ice sheets deform the solid Earth and sea surface. Altering bedrock topography and sea levels at the grounding line, GIA exerts a strong control on marine ice sheet dynamics, especially on the multi-century timescales to be considered in ISMIP7 (Ice Sheet Model Intercomparison Project for the Coupled Model Intercomparison Project - Phase 7). To accurately capture bedrock and sea level changes, ice sheet models must be coupled with GIA models that include realistic spatial variations in solid Earth structure. However, GIA models that incorporate 3-D variations in Earth structure are computationally expensive, limiting their use in ice sheet modelling. Consequently, most ice sheet models still assume rigid bedrock topography or rely on simple GIA models that neglect realistic lateral variations in Earth structure. Here, we assess the performance of FastIsostasy, a computationally-efficient regional 2-D GIA model, relative to Seakon, a state-of-the-art 3-D GIA model, in iteratively coupled ice sheet – GIA simulations of Antarctic Ice Sheet evolution over the next five centuries. Coupled simulations that employ FastIsotasy produce GIA, ice thickness, and grounding line predictions that closely match those from simulations using Seakon, and, more specifically, perform better than ice sheet simulations that rely on overly simplified GIA models. With the protocols for ISMIP7 under active development, FastIsostasy offers a viable approach for ice sheet modellers to accurately and efficiently capture solid Earth – ice sheet feedbacks, permitting improved projections of Antarctic ice mass change and associated sea level contributions over the coming centuries.

1 Introduction

The Antarctic Ice Sheet (AIS) is projected to become the dominant and most uncertain contributor to sea level rise over the coming centuries (Fox-Kemperer et al., 2021). AIS evolution will depend on a variety of factors, including bedrock elevation

https://doi.org/10.5194/egusphere-2026-2640
Preprint. Discussion started: 11 June 2026

changes beneath the ice and sea level changes at the grounding line (Gomez et al., 2010, 2012, 2015; Konrad et al., 2015; Larour et al., 2019; Coulon et al., 2021). Several recent studies adopting coupled ice sheet - glacial isostatic adjustment (GIA) models (also referred to as coupled ice sheet - sea level models) have demonstrated the importance of accounting for realistic 3-D variability in solid Earth structure in projections of AIS evolution (Gomez et al., 2024; van Calcar et al., 2025), where GIA is defined as the gravitational, rotational and deformational response of the solid Earth to ice and water mass redistribution at the surface. Upper mantle viscosities are estimated to vary by up to ca. 5 orders of magnitude across Antarctica (e.g. Kaufmann et al., 2005; Ivins et al., 2022; Hazzard et al., 2023; Gomez et al., 2024) and lithospheric thickness varies by ca. $100 - 200\,\mathrm{km}$ between West and East Antarctica (Shen et al., 2018; Lloyd et al., 2020; Wiens et al., 2023; Hazzard et al., 2023; Brown and Fischer, 2025). Accurately representing solid Earth structure in GIA models coupled to ice sheet models has shown to be especially important in modelling future ice sheet retreat in West Antarctica (Konrad et al., 2015; Larour et al., 2019; Gomez et al., 2024; van Calcar et al., 2025), a region where upper mantle viscosities are estimated to reach as low as $10^{18}\,\mathrm{Pa\,s}$ (Nield et al., 2014; Zhao et al., 2017; Barletta et al., 2018; Nield et al., 2018; Samrat et al., 2020, 2021; Ivins et al., 2022; Nield et al., 2025). These low viscosities result in rapid viscous deformation on decadal to centennial timescales (e.g. Barletta et al., 2018; Larour et al., 2019; Powell et al., 2020; Coulon et al., 2021; Wan et al., 2022; Nield et al., 2025; Gomez et al., 2024; Lucas et al., 2025), and the amplitude of this deformation is further enhanced in regions with thinner lithosphere (Nield et al., 2018).

Despite growing recognition of the importance of accurately representing bedrock elevation and sea level change, most ice sheet models still assume a rigid bed (i.e., no bedrock adjustment to ice load changes) or compute bedrock elevation changes from simple GIA models. Only four of the sixteen ice sheet models participating in the most recent Ice Sheet Model Intercomparison Project - Phase 6 (ISMIP6; Nowicki et al., 2016) accounted for bedrock adjustment in simulations through 2300, while the remaining models assumed a rigid bed (Seroussi et al., 2024). The four ice sheet models participating in ISMIP6 that did account for bedrock adjustment adopted either an elastic lithosphere - relaxed asthenosphere model (ELRA; Le Meur and Huybrechts, 1996) or an elastic lithosphere - viscous asthenosphere model (ELVA; Cathles, 1975; Lingle and Clark, 1985; Bueler et al., 2007). The ELRA and ELVA models are commonly adopted by ice sheet modellers because they are capable of approximating the viscoelastic behaviour of the solid Earth at a low computational cost (DeConto and Pollard, 2016; Pattyn, 2017; Lipscomb et al., 2019; Rückamp et al., 2019; Robinson et al., 2020). However, standard implementations of ELRA and ELVA are incapable of (1) accounting for lateral variations in solid Earth structure and (2) accurately computing the gravitational and rotational feedbacks of ice mass change on sea level. Adaptions of the ELRA model have been developed to represent large-scale lateral variations in Earth structure between West and East Antarctica and, additionally, to approximate geoid changes (Coulon et al., 2021), yet such approaches still rely on a simplified treatment of Earth deformation and have seen only limited application in ice sheet models.

With ISMIP7 (Ice Sheet Model Intercomparison Project for the Coupled Model Intercomparison Project - Phase 7) in active development, an opportunity arises to better represent bedrock elevation changes in ice sheet models. 3-D GIA models, which incorporate realistic lateral and radial variations in Earth structure, are the best option for accurately modelling future bedrock and sea level changes in Antarctica; however, they are too computationally expensive to be widely implemented in ice sheet models. FastIsostasy, a regional 2-D GIA model, bridges the gap between simple, computationally cheap GIA

https://doi.org/10.5194/egusphere-2026-2640
Preprint. Discussion started: 11 June 2026

models commonly used by ice sheet modellers and computationally expensive 3-D GIA models (Swierczek-Jereczek et al., 2024). FastIsostasy takes into account the laterally-variable properties of the solid Earth and approximates the deformational and gravitational response to changes in surface loading with minimal computational expense. Furthermore, FastIsostasy has performed well in benchmarks against the state-of-the-art Seakon 3-D GIA model (Latychev et al., 2005), including idealized simulation examples as well as a simulation over the last glacial cycle with loading from ICE_6GD (Peltier et al., 2018).

In this study, we assess the performance of FastIsostasy versus Seakon in iteratively coupled ice sheet - GIA simulations of AIS evolution over the next five centuries. Projections of AIS evolution facilitate model comparison but are not the primary objective of this study. This work instead serves as a reference for ice sheet modellers who intend to use FastIsostasy in order to improve their representation of the GIA response at low computational cost.

2 Methods

We start by describing the coupling procedure and then proceed to discuss the adopted GIA models, the Earth models used in the GIA models, and the ice sheet model in further detail. In this study, we employ an iterative ice sheet - GIA coupling approach that has previously been applied to model AIS evolution over the last deglaciation (Gomez et al., 2018) and the next ca. 500 years (Gomez et al., 2024). As this iterative coupling approach is fully described in (Gomez et al., 2018, 2024), we only summarize the approach here. To start the coupling, ice thickness changes are simulated using the PSUICE3D ice sheet model (Pollard and DeConto, 2012, 2020) with 1-year time stepping from 1950 to 2500. In this initial ice sheet simulation, bed elevation changes are accounted for using an ELRA model (Pollard and DeConto, 2012). The GIA models then compute either regional (FastIsostasy) or global (Seakon) GIA changes offline, using ice thickness field from PSUICE3D at 2-year time steps from 1950 to 2500. Changes in bedrock and sea surface elevation computed using the GIA models are linearly interpolated to 1-year time increments before being passed back to the ice sheet model. The coupling procedure is repeated four to five times until the predicted ice volume change converges (Figs. S2-S3). Throughout the main text, we only present and discuss results from the final iteration of the coupled ice sheet - GIA simulations. Results showcasing select intermediate iterations can be found in the Supplementary Material (Figs. S2-S3).

The initial bed topography in Antarctica is taken from Bedmap2 (Fretwell et al., 2013) and, north of 60°S, from the Global Relief Model ETOPO 2022 (NOAA National Centers for Environmental Information, 2022). Results from the iterative coupling approach have been shown to be comparable to those produced by the standard interactive coupling procedure (Gomez et al., 2013), in which the GIA model is called to update the ice sheet model's bed topography at regular coupling time intervals during the simulation.

2.1 FastIsostasy 2-D regional GIA model

FastIsostasy is a 2-D regional GIA model that relies on Fast-Fourier Transforms (FFTs) to efficiently compute the deformational and gravitational GIA response. Unlike Seakon, FastIsostasy omits the rotational response, since the regional nature of its domain intrinsically prevents this computation. Compared to gravitation and deformation, rotational effects have been found

https://doi.org/10.5194/egusphere-2026-2640
Preprint. Discussion started: 11 June 2026

to be negligible for future AIS projections (Larour et al., 2019), and we do not expect this discrepancy to have a significant impact on coupled simulation results.

The ice thickness field, as computed by the ice sheet model, is passed to FastIsostasy, which returns the updated bedrock elevation, z_b, and relative sea level, S, computed as:

$$z_b(x,y,t) = z_b^{\text{ref}}(x,y) + u_v(x,y,t) + u_e(x,y,t) \tag{1}$$

$$S(x,y,t) = z_{ss}(x,y,t) - z_b(x,y,t) \tag{2}$$

$$z_{ss}(x,y,t) = s(t) + \Delta z_{ss}(x,y,t) \tag{3}$$

with z_b^{ref}, the reference bed elevation; u_v and u_e, the viscous and elastic vertical bedrock displacement, respectively; z_{ss}, the sea surface elevation; $s(t)$, the barystatic sea level; and $\Delta z_{ss}(x,y,t)$, the perturbation of sea surface elevation. The barystatic sea level is computed according to differences in the ice thickness above flotation, taking into account a density and bedrock correction following Goelzer et al. (2020). The perturbation of sea surface elevation and the elastic bedrock displacement are computed by convolving the anomalies of mass columns with suitable Green's functions, following Bueler et al. (2007) and Coulon et al. (2021), respectively. Finally, the time derivative of the viscous displacement is given by:

$$\partial_t u_v = \mathcal{F}^{-1}\left(\frac{1}{\kappa}\mathcal{F}\left(\frac{AF}{2\eta}\right)\right), \quad \text{with:} \tag{4}$$

$$F = p + \partial_{xx}M_{xx} + 2\,\partial_{xy}M_{xy} + \partial_{yy}M_{yy}, \tag{5}$$

$$M_{xx} = -D\left(\partial_{xx}u_v + \nu\partial_{yy}u_v\right), \tag{6}$$

$$M_{yy} = -D\left(\partial_{yy}u_v + \nu\partial_{xx}u_v\right), \tag{7}$$

$$M_{xy} = -D\,(1-\nu)\,\partial_{xy}u_v. \tag{8}$$

Here, $\eta = \eta(x,y)$ is the effective viscosity field; $D = D(x,y)$, the lithospheric rigidity field; ν, the Poisson ratio of the upper mantle; κ, the pseudo-differential operator transformed into Fourier space (Bueler et al., 2007); $\mathcal{F}$, the forward FFT and $\mathcal{F}^{-1}$ its inverse. The active mask, A, yields 0 far away from the ice sheet and 1 otherwise (Fig. 1). Thus, the evolution of the ocean load and the bedrock displacement are coupled to each other within an area that covers the continental shelf break but not beyond. This is needed to impose an average displacement that yields zero at the border (Bueler et al., 2007). Once discretised on a regular grid, the derivatives are approximated via finite differences and Eq. 4 becomes an ODE of dimension $n = n_x \times n_y$, which is integrated forward in time via a third-order Bogacki-Shampine scheme with adaptive time stepping. The evaluation of the right-hand side relies on FFTs, therefore scaling with the problem dimension as $\mathcal{O}(n \log n)$. It is therefore much cheaper to solve than the typical PDE of dimension $n = n_x \times n_y \times n_z$ that arises in 3-D GIA codes and is usually solved via a linear solver that scales as $\mathcal{O}(n^3)$. We emphasise that FastIsostasy was not developed to replace 3-D GIA models, but rather to approximate them at low computational cost in order to improve the representation of gravitational and deformational feedbacks on ice sheet dynamics.

https://doi.org/10.5194/egusphere-2026-2640
Preprint. Discussion started: 11 June 2026

2.2 Seakon 3-D global GIA model

Seakon is a 3-D global GIA model that uses a finite volume scheme for forward computation of viscoelastic deformation (Latychev et al., 2005) and is capable of regional grid refinement (Gomez et al., 2018). Seakon solves the sea level equation allowing for shoreline migration (Kendall et al., 2005) and computes the response of a self-gravitating, elastically compressible Earth to a specified loading history while accounting for Earth rotational effects (Milne and Mitrovica, 1998; Mitrovica and Milne, 2003; Mitrovica et al., 2005). The computational grid adopted for the Seakon simulations has a lateral surface resolution of ca. $10\,\mathrm{km}$ over the AIS and $12-15\,\mathrm{km}$ globally outside of Antarctica. Lateral resolution in the computational grid decreases with depth, with a resolution of ca. $50\,\mathrm{km}$ at the core-mantle boundary. The radial layers of the computational grid are constructed to adhere to discontinuities in the material properties of the STW105 seismic reference model (Kustowski et al., 2008), with the shallowest layers at 12, 24, and $43\,\mathrm{km}$ depth.

2.3 Earth models

Seismic imaging and regional GIA studies indicate that solid Earth structure varies strongly across Antarctica. East Antarctica is underlain by thick (ca. $150-250\,\mathrm{km}$) Precambrian lithosphere that thins towards the coast and sublithospheric upper mantle seismic velocities not far removed from the global average (e.g Ritzwoller et al., 2001; Lloyd et al., 2020; Wiens et al., 2023; Chua and Lebedev, 2025; Hansen and Emry, 2025). In contrast, West Antarctica is more tectonically active with thinner lithosphere (ca. $50-125\,\mathrm{km}$; e.g. An et al., 2015; Wiens et al., 2023; Brown and Fischer, 2025) that is underlain by localized regions of seismically slow and presumably warm sub-lithospheric mantle associated with plumes, hotspots, slab windows, and zones of more recent Cenozoic extension (e.g. Lloyd et al., 2020; Lucas et al., 2020, 2021; Chua and Lebedev, 2025). In these areas, regional GIA studies report very low upper mantle viscosities ($10^{18}-10^{19}\,\mathrm{Pas}$; Nield et al., 2014; Zhao et al., 2017; Barletta et al., 2018; Samrat et al., 2021; Nield et al., 2023), while between these regions globally average upper mantle viscosities ($10^{20}-10^{21}\,\mathrm{Pas}$, e.g., Nield et al., 2016) are found and correlate with seismic velocities near the global average (e.g. Lloyd et al., 2020; Chua and Lebedev, 2025). This strong heterogeneity directly impacts the spatial dependence of GIA observables on mantle viscosity, in which a single point observation in Antarctica strongly depends on the assumed viscosity structure in the upper mantle and upper-lower mantle over a region roughly the size of West Antarctica (Lloyd et al., 2024). Thus, for both global and regional GIA simulations, there is a need for high-resolution 3-D viscosity models that span broad regions and extend into the lower mantle.

Together, seismically-inferred and GIA-imaged mantle viscosities indicate that solid Earth response time to ice sheet change varies from years to tens of thousands of years across the Antarctic continent. The magnitude and wavelength of the solid Earth response is further modulated by substantial variations in lithospheric thickness (ca. $50-200\,\mathrm{km}$) across Antarctica. Capturing the variability of this response is essential for improving models of marine-based ice sheets, in which regions of rapid uplift (e.g., Amundsen Sea Embayment) have the potential to stabilize or slow grounding line retreat, while regions with a slower response (e.g., Wilkes Subglacial Basin) may undergo more rapid retreat (Larour et al., 2019; Gomez et al., 2024; van Calcar et al., 2025).

https://doi.org/10.5194/egusphere-2026-2640
Preprint. Discussion started: 11 June 2026

To capture the highly variable solid Earth response in Antarctica, we run coupled ice sheet-GIA simulations using two 3-D viscoelastic models developed from recent constraints on solid Earth structure. These Earth models capture a wide range of plausible mantle viscosities inferred from geodetic observations and seismic imaging across Antarctica and will be referred to as the "strong" and "weak" Earth models, respectively. Lateral viscosity variability in both the strong and weak Earth models is inferred from the ANT-20 seismic shear-wave speed model in Antarctica (Lloyd et al., 2020) and the GLAD-M25 seismic shear-wave speed model globally (Lei et al., 2020). The procedures used to construct the Earth models and convert 3-D seismic wave speed variations to viscosity differ between the strong and weak Earth models, as detailed in the following.

2.3.1 Strong Earth model

We construct the strong Earth model from inferences of steady-state diffusion creep viscosity (Hazzard et al., 2023; Lloyd et al., 2024), in which the upper mantle viscosity is calibrated following Richards et al. (2020). It is worth noting that these inferred viscosities tend to be higher than those observed in regional GIA studies, an observation that has been interpreted to indicate the need for transient rheology (Hazzard et al., 2023). In this context, the Maxwell viscosities determined by GIA studies may be viewed as time-dependent apparent viscosities (Lau et al., 2021) and, in our case, serve as calibration targets for the weak Earth model (Section 2.1.2). In the transition zone and lower mantle, the viscosity inferences are based on both ANT-20 ($400 - 800\,\mathrm{km}$ depth) and GLAD-M25, following the approach first presented in Austermann et al. (2021).

To obtain the global 3-D viscosity model required by Seakon, we embed the ANT-20 inference into the global GLAD-M25 inference by applying a linear correction to the GLAD-M25 viscosities, as well as a combination of geographic and "data density" weighting in order to ensure a smooth transition between the two models (Fig. S1). The linear correction is determined and applied to GLAD-M25 for each overlapping depth of the two models, with this correction ensuring a linear fit of $\eta_{\text{GLAD-M25}}$ with respect to $\eta_{\text{ANT-20}}$ that lies on a 1:1 line. Geographic weights, w_g, range from 0 to 1 with: (1) all ANT-20 weights north of the mesh boundary being 0, (2) ANT-20 weights increasing linearly from 0 to 1 from the mesh boundary to 5 degrees inside of the boundary, and (3) ANT-20 weights of 1 further inside the mesh boundary. The "data density" weighting, w_d, is based on the pseudo-Hessian, which serves as a proxy for data density and is used to balance the gradient in the ANT-20 tomographic inversion (Lloyd et al., 2020). Here we smooth the pseudo-Hessian from the final iteration of the tomographic inversion using a 3-D Gaussian filter with a standard deviation of $150\,\mathrm{km}$ laterally and $5\,\mathrm{km}$ radially. Weights, w_d, are determined in $\log_{10}$ space as described in Table 1. In the uppermost mantle, the majority of the ANT-20 model space has a weight of 1, and acceptable regions of the ANT-20 model narrows as the model descends to deeper depths. The total weight assigned to the ANT-20 viscosity inference is $w_t = w_g \cdot w_d$ and weights assigned to the GLAD-M25 viscosity inferences are $1 - w_t$. Thus, at any given location, $\boldsymbol{x}$, the merged model viscosity is $\eta(\boldsymbol{x}) = w_t(\boldsymbol{x}) \cdot \eta_{\mathrm{ANT-20}}(\boldsymbol{x}) + (1 - w_t(\boldsymbol{x})) \cdot \eta_{\mathrm{GLAD-M25}}(\boldsymbol{x})$. For the final merged model, the volumetric mean is $\sim 3 \times 10^{20}\,\mathrm{Pa\,s}$ in the sub-lithospheric upper mantle and $\sim 5 \times 10^{21}\,\mathrm{Pa\,s}$ in the lower mantle.

https://doi.org/10.5194/egusphere-2026-2640
Preprint. Discussion started: 11 June 2026

Table 1. Data density weighting and empirically derived values of $\log_{10} P_s$

	$w_d = 0$	Linear scales to $w_d\,(0 \to 1)$	$w_d = 1$
Upper mantle $(0 - 400\,\mathrm{km})$	$\log_{10} P_s < -2.0$	$\log_{10} P_s \in [-2.0, -1.75]$	$\log_{10} P_s > -1.75$
Transition zone & lower mantle $(400 - 800\,\mathrm{km})$	$\log_{10} P_s < -2.25$	$\log_{10} P_s \in [-2.25, -2.0]$	$\log_{10} P_s > -2.0$

2.3.2 Weak Earth model

We also complete coupled ice sheet-GIA simulations using a weak Earth model, which is characterized by a lower viscosity upper mantle across most of Antarctica compared to the strong Earth model (Figs. 1, S1). The weak Earth model is similar to the Earth model adopted in Gomez et al. (2024), but differs in that global viscosity variations are inferred from GLAD-M25 (Lei et al., 2020) rather than S362ANI (Kustowski et al., 2008). The weak Earth model is constructed by estimating variations in mantle viscosity from relative variations in seismic velocity, following Austermann et al. (2013). Viscosity variations are based on the ANT-20 seismic shear-wave seismic model (Lloyd et al., 2020) between the base of the lithosphere and 670-km depth in the region south of 47°S and the GLAD-M25 global shear-wave seismic model elsewhere (Lei et al., 2020). The lateral variations in mantle viscosity are superimposed onto a 1-D reference viscosity profile, which has viscosities of $10^{20}\,\mathrm{Pa\,s}$ and $5 \cdot 10^{21}\,\mathrm{Pa\,s}$ in the upper mantle (from bottom of lithosphere to 670-km depth) and lower mantle (from 670-km depth to the core-mantle boundary), respectively. In the approach of converting from seismic velocities to viscosity, a scaling factor (ϵ) is adopted in the conversion of temperature to viscosity variations. Here we adopt fixed scaling factors of $0.033\,\mathrm{K}^{-1}$ in Antarctica and $0.04\,\mathrm{K}^{-1}$ globally, consistent with (Gomez et al., 2024). Following Wan et al. (2022), the scaling factors were calibrated to best reflect absolute upper mantle viscosity estimates inferred from GNSS observations in the northern Antarctic Peninsula (Nield et al., 2014), the Fleming Glacier in the central Antarctic Peninsula (Zhao et al., 2017), and the Amundsen Sea Embayment (Barletta et al., 2018).

2.3.3 2-D Earth models for FastIsostasy

FastIsostasy requires the derivation of a 2-D viscosity field from a given 3-D viscosity field, an exercise that we henceforth refer to as "viscosity lumping". To this end, Swierczek-Jereczek et al. (2024) defined a layered structure of the solid Earth over which an induction can be performed–a formula that is however limited to homogenous viscosity. Finding a physics-based lumping into a 2-D effective viscosity that yields the smallest error compared to a 3-D GIA model, therefore, remains an open question. For the present work, we tested various heuristic lumping techniques. A comparison of the obtained results is provided in the Supplementary Material and shows that the lumping with the smallest maximal error is obtained by using the minimum viscosity over a reference depth of $150\,\mathrm{km}$ below the lithosphere-asthenosphere boundary (LAB). This exploration of the viscosity lumping is empirical but can nonetheless be interpreted physically: the lowest viscosity of the upper mantle, i.e., the region that flows the fastest, dominates the flow. The resulting viscosity fields for the strong and weak Earth models are shown in Fig. 1.

https://doi.org/10.5194/egusphere-2026-2640
Preprint. Discussion started: 11 June 2026

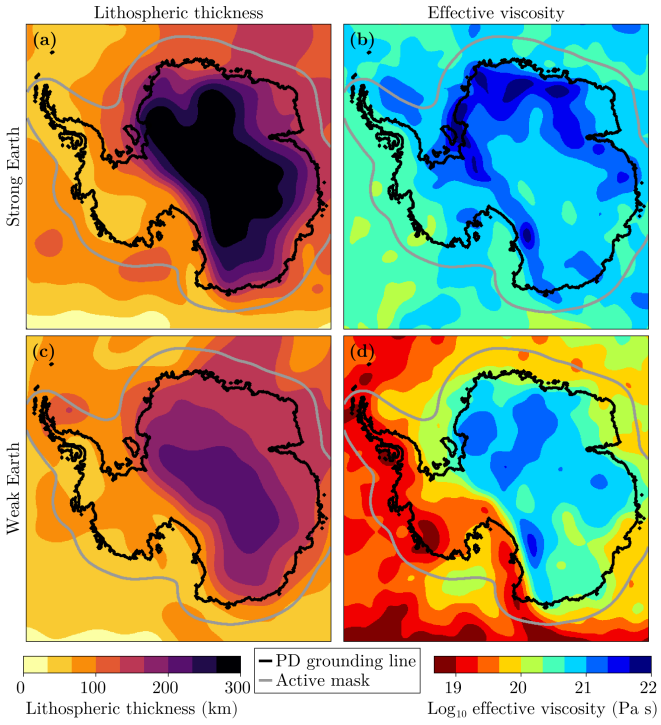

Figure 1. FastIsostasy Earth models. (a-b) Strong and (c-d) weak Earth models used in FastIsostasy, after "lumping" the 3-D viscosity model as described in the Supplementary Material. Changes in surface load are allowed within the active mask and are set to zero outside of the mask. Depth slices of the strong and weak Earth models used in Seakon are shown in Figure S1. Black lines show the initial grounding line position in 1950, while grey lines outline the active mask.

2.4 PSUICE3D ice sheet model

We simulate the AIS dynamics using the PSUICE3D ice sheet/shelf model, which employs a hybrid combination of shallow-ice and shallow-shelf approximations at a horizontal resolution of 10 km (Pollard and DeConto, 2012, 2020). The simulations of the AIS evolution start from a modern state in 1950 and run until 2500, with 1 year time steps. Our simulations adopt the same atmospheric and oceanic forcings as those detailed in DeConto et al. (2021) for Representative Concentration Pathways 2.6 and 8.5 (respectively RCP2.6 and RCP8.5; Meinshausen et al., 2011). We perform ice sheet simulations incorporating both the marine-ice sheet instability mechanism (MISI) and marine ice cliff instability mechanism (MICI, Pollard et al., 2015). More specifically, we simulate ice sheet evolution under RCP8.5 with MICI (RCP8.5-MICI), RCP8.5 with only MISI (RCP8.5-MISI), and RCP2.6 with only MISI (RCP2.6-MISI). Invoking MICI results in substantially greater ice loss compared to other multi-century simulations (e.g. Seroussi et al., 2024), producing a large GIA response that more difficult to fit by a regional GIA model and, therefore, useful for evaluating the performance of coupled simulations with FastIsostasy versus Seakon. The initial conditions of the ice-sheet model (ice thickness, bed elevation, velocity, basal sliding coefficients, and internal ice and

https://doi.org/10.5194/egusphere-2026-2640
Preprint. Discussion started: 11 June 2026

bed temperature) are obtained from a 100,000 year spin-up with observed climate forcing and correspond to those used by DeConto et al. (2021) and Gomez et al. (2024).

In the initial step of our coupled procedure, we compute bed deformation in PSUICE3D using an ELRA model, which consists of a local elastic layer and an asthenosphere that relaxes with a single constant relaxation time. Typically, a relaxation time of $\tau = 3000\,\mathrm{yr}$ is adopted in PSUICE3D and in other ice sheet models (e.g. Le Meur and Huybrechts, 1996; Pollard and DeConto, 2012; Lipscomb et al., 2019; Robinson et al., 2020). However, van Calcar et al. (2026) find that an ELRA model with $\tau = 500\,\mathrm{yr}$ best approximates the sea level contribution in ice sheet simulations adopting a 3-D GIA model for projections until the year 2500. Motivated by these findings, we evaluate the performance of our Seakon and FastIsostasy coupled simulations versus standalone PSUICE3D simulations with $\tau = 500\,\mathrm{yr}$ and $\tau = 3000\,\mathrm{yr}$ in the ELRA model. In addition, van Calcar et al. (2026) proposed a simple relationship between the average viscosity in the topmost part of the upper mantle and the effective relaxation time. Thus, 2-D fields of the relaxation time can be derived from the 3-D viscosity, which result in a laterally-variable formulation of ELRA (LV-ELRA) that provides a much better approximation than using a single relaxation time. This is a promising approach because it requires minimal implementation and coupling effort, yet it has not been widely adopted to date. Therefore, we compare the results of FastIsostasy to ELRA500 and ELRA3000 in the main part of the manuscript (Figs. 4, S4-S10), but show a complementary analysis with LV-ELRA in the Supplementary Material (Fig. S11-S14).

3 Results

The primary objective of this analysis is to compare the performance of FastIsostasy versus Seakon in capturing the gravitational and deformational response to Antarctic ice mass changes on multi-century timescales in coupled ice sheet - GIA simulations adopting the strong and weak Earth models. We start by comparing ice thickness and grounding line predictions between simulations adopting FastIsostasy versus Seakon and continue to a more detailed discussion of vertical deformation and sea surface height predicted by the coupled simulations.

3.1 Ice thickness and grounding line predictions

Overall, we find a good match of ice thickness and grounding line projections between the Seakon and FastIsostasy coupled simulations for all climate forcing and Earth model combinations (Figs. 2-4, S4-S15). Average differences in ice thickness across the AIS between coupled simulations adopting FastIsostasy versus Seakon under RCP8.5-MICI reach $21\,\mathrm{m}$ and $32\,\mathrm{m}$ in the year 2500 for the strong and weak Earth, respectively (Fig. 2.a). Average ice thickness differences between Seakon and FastIsostasy coupled simulations are even lower under RCP8.5-MISI and RCP2.6-MISI, reaching a maximum of only $\sim 2.4\,\mathrm{m}$ by 2500 (Figs. 3, S8-S10). In 2150, the difference between the FastIsostasy and Seakon coupled simulations is lower still, reaching $9\,\mathrm{m}$, $0.7\,\mathrm{m}$, and $0.5\,\mathrm{m}$ in the RCP8.5-MICI, RCP8.5-MISI, and RCP2.6-MISI scenarios, respectively. Over the duration of the coupled simulations, grounding line positions differ only minimally between simulations adopting FastIsostasy versus Seakon (Figs. 4, S8, S10). Generally, the differences in ice thickness and grounding line position between the FastIsostasy and Seakon simulations increase with increasing magnitude of ice load change.

https://doi.org/10.5194/egusphere-2026-2640
Preprint. Discussion started: 11 June 2026

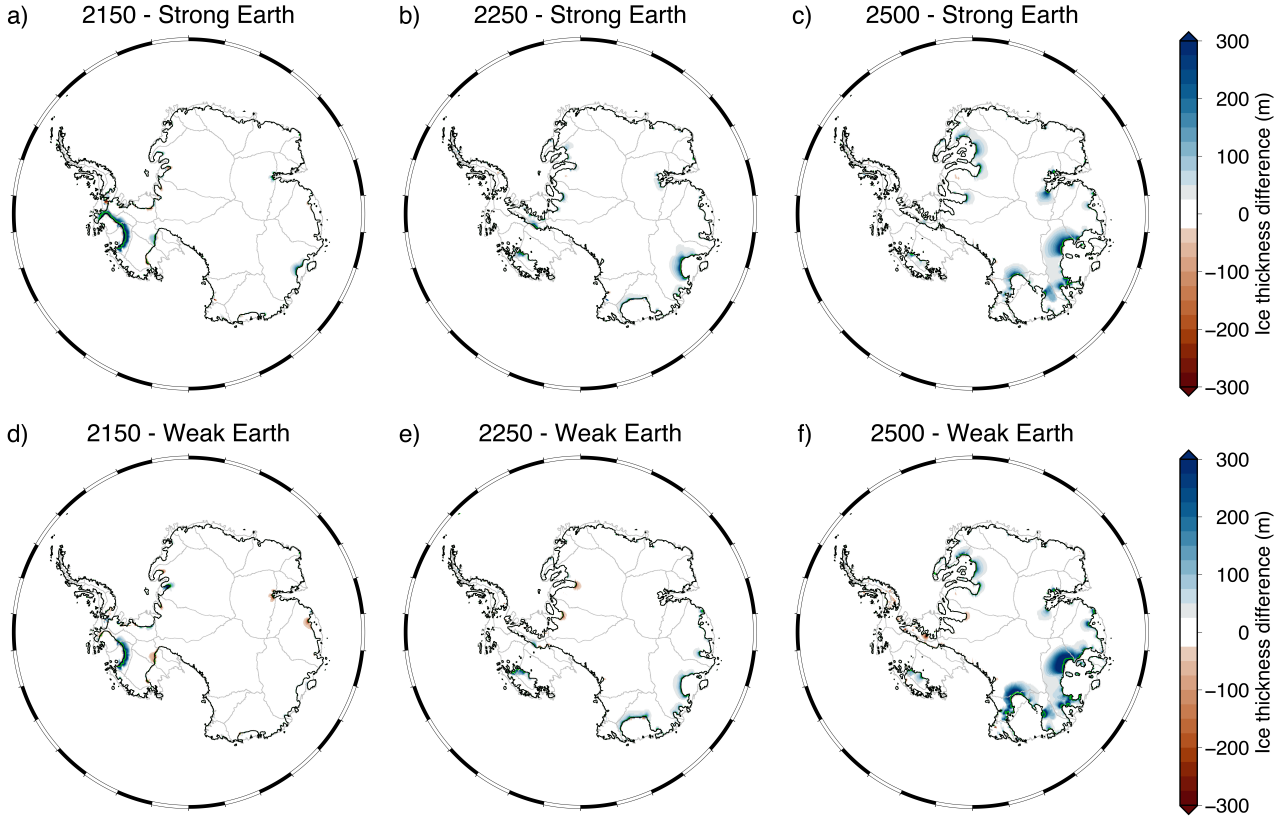

Figure 2. Differences between Seakon and FastIsostasy ice sheet projections for RCP8.5-MICI. Differences in ice thickness and grounding line projections at years 2150, 2250, and 2500 between Seakon and FastIsostasy simulations for RCP8.5-MICI (a-c) for the strong Earth model and (d-f) for the weak Earth model (i.e., Seakon minus FastIsostasy). Grounding line positions from Seakon and FastIsostasy simulations are shown in black and green, respectively. Note that the grounding lines from Seakon and FastIsostasy largely overlap. Glacial basins are outlined in gray (Zwally et al., 2012).

To assess the performance of FastIsostasy relative to ELRA models, we additionally compare our ice thickness predictions with results from standalone PSUICE3D simulations using relaxation times of 500 and 3000 years (ELRA500, ELRA3000; Figs. 4, S4-S10). In 2500 under RCP8.5-MICI, the ELRA3000 model yields a mean error in ice thickness of $74\,\mathrm{m}$ and $107\,\mathrm{m}$ for the strong and weak Earth, respectively (Fig. 4.a). This is about three times more than the error obtained when using
255 FastIsostasy. The analysis of van Calcar et al. (2026) indicates that an ELRA model with $\tau = 500\,\mathrm{yr}$ provides the closest approximation to AIS sea level contributions estimated in coupled simulations adopting a 3-D GIA model over timescales exceeding 400 years. In 2500 under RCP8.5-MICI, the ELRA500 model yields mean ice thickness errors of $25\,\mathrm{m}$ and $57\,\mathrm{m}$ for the strong and weak Earth models, respectively. This is about $1.2 - 1.8$ times more than the error obtained when using FastIsostasy (Fig. 4.a). A similar behaviour of the error arises for RCP8.5-MISI and RCP2.6-MISI (Figs. S6-S14).

https://doi.org/10.5194/egusphere-2026-2640
Preprint. Discussion started: 11 June 2026

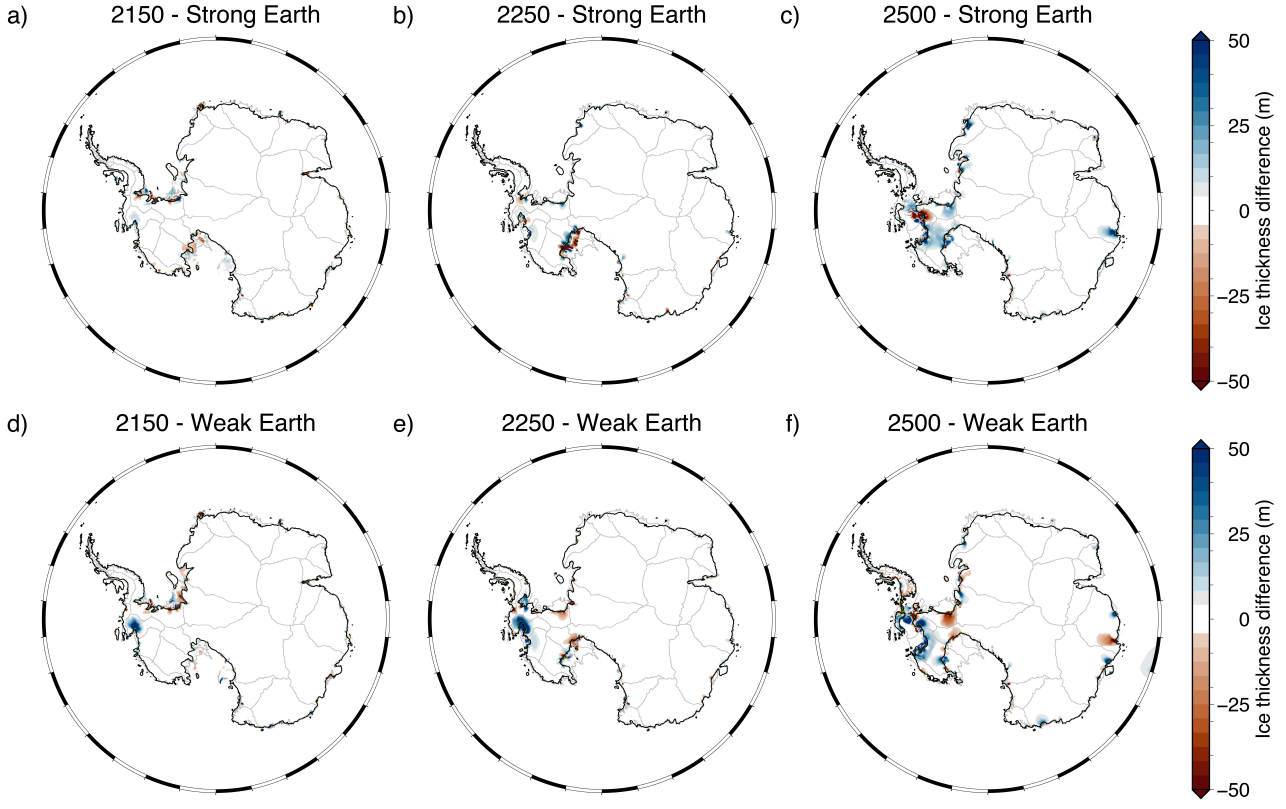

Figure 3. Differences between Seakon and FastIsostasy ice sheet projections for RCP8.5-MISI. Differences in ice thickness and grounding line projections at years 2150, 2250, and 2500 between Seakon and FastIsostasy simulations for RCP8.5-MISI (a-c) for the strong Earth model and (d-f) for the weak Earth model (i.e., Seakon minus FastIsostasy). Grounding line positions from Seakon and FastIsostasy simulations are shown in black and green, respectively (barely distinguishable due to overlap).

3.2 GIA model predictions

To understand the close match of projected ice thickness between the Seakon and FastIsostasy coupled simulations, we evaluate output from each GIA model in more detail. For the strong Earth model, the patterns of vertical bedrock displacement and sea surface height perturbation at year 2500 with respect to year 1950 are very similar between the two models (Fig. 5.a & d; Fig 5.b & e). The absolute error of the resulting RSL prediction has mean and maximal values of about 4 and 22 m between the FastIsostasy and Seakon coupled simulations, respectively (Figs. S11-S12). In addition to the accurate match at year 2500, the time-dependent behaviour of FastIsostasy at some sampled locations largely agrees with Seakon (Fig. 5.c & e), resulting in error metrics that only grow marginally over time (Fig. S12). The trends in sea surface height perturbation and vertical displacement in the FastIsostasy simulations are similar to those found in the Seakon simulations (Fig. 5.c), except for the peripheral forebulge region (Fig. 5.c, black curve). This is an expected result, since FastIsostasy tends to underestimate the

https://doi.org/10.5194/egusphere-2026-2640
Preprint. Discussion started: 11 June 2026

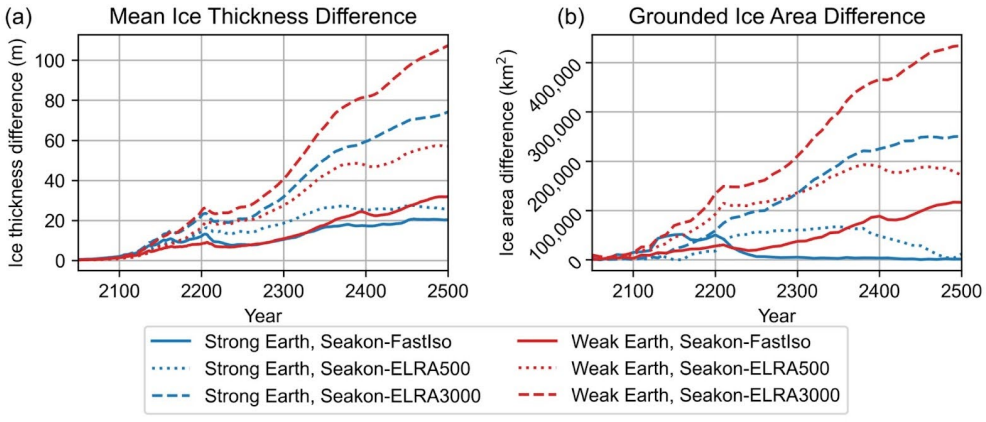

Figure 4. Comparing differences in ice sheet thickness and grounded area between simulations adopting Seakon versus those adopting FastIsostasy, ELRA500, and ELRA3000. Difference in (a) mean grounded ice thickness and (b) grounded area extent between simulations adopting FastIsostasy, ELRA500, and ELRA3000 with respect to those adopting Seakon for the RCP8.5-MICI scenario.

forebulge deformation (Swierczek-Jereczek et al., 2024). This misrepresentation is, however, largely irrelevant for ice retreat, as demonstrated by the close match in ice thickness (Figs. 2-3).

Compared to the coupled simulations using the strong Earth model, the vertical bedrock displacement is greater in both the FastIsostasy and Seakon coupled simulations with the weak Earth model, yielding values up to three times larger in West Antarctica and twice as large in East Antarctica (Figs. 5-6). This discrepancy stems from viscosity values that are greatly reduced in the west and somewhat reduced in the east compared to the strong Earth model (Figs. 1, S1). In contrast, the gravitational response is smaller in simulations with the weak Earth model, which is due to the faster compensation of mass anomalies associated with rapid viscous uplift. As in the simulations with the strong Earth model, both vertical displacement and sea surface height perturbations exhibit similar patterns in the Seakon and FastIsostasy simulations with the weak Earth model. The most pronounced discrepancies again occur in the forebulge region, but these do not preclude close agreement in the predicted ice retreat, which mainly occurs away from the forebulge (Figs. 2-3).

The discrepancies between simulations adopting the strong and weak Earth models using Seakon are much larger than between those between Seakon and FastIsostasy using the same Earth model. In other words, the parametric uncertainty of the solid Earth is larger than the discrepancy between FastIsostasy and the Seakon 3-D GIA model. Thus, improving the representation of the GIA response in future projections of sea level does not require the use of GIA models that are more complex than FastIsostasy but, instead, requires improved constraints on solid Earth properties.

To compare the combined effect of the deformational and gravitational response among models, the RSL anomaly at year 2500 with respect to year 1950 is shown in the Supplementary Material (Figs. S11 & S13). Whereas the RSL pattern is barely distinguishable between FastIsostasy and Seakon, all other models fail to reproduce the RSL pattern predicted by Seakon. Consistent with Coulon et al. (2021) and van Calcar et al. (2026), the RSL pattern obtained by ELRA improves when using

https://doi.org/10.5194/egusphere-2026-2640
Preprint. Discussion started: 11 June 2026

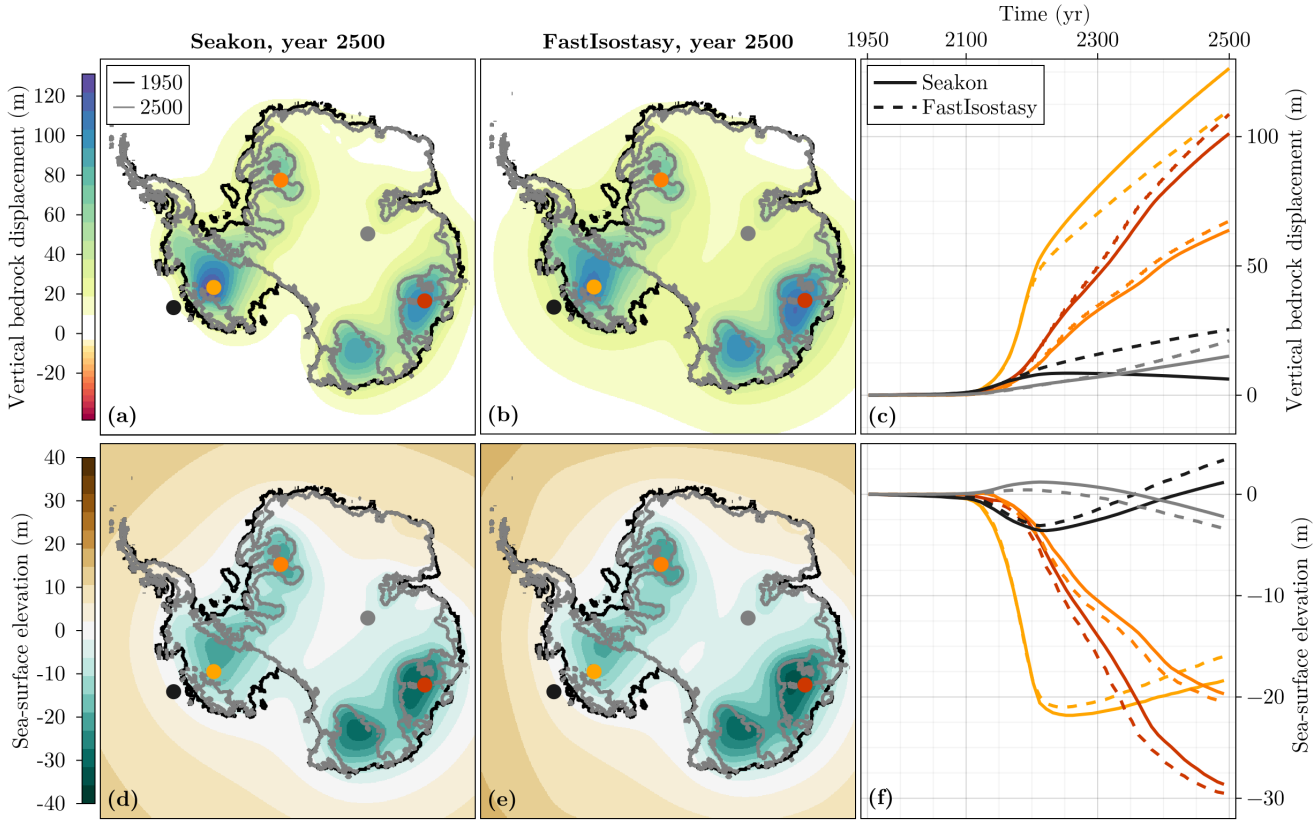

Figure 5. Comparison of GIA predictions using the strong Earth model. Anomaly of (a-b) vertical bedrock displacement and (d-e) sea surface elevation at year 2500 with respect to year 1950 from Seakon and FastIsostasy coupled simulations with the strong Earth model. Transient (c) bedrock displacement and (f) sea surface height (SSH) perturbation of the points highlighted in shades of gray and orange in (a,b,d,e).

2-D fields of the relaxation time (LV-ELRA), however, with error metrics that are consistently larger than those of FastIsostasy (Figs. S12 & S14). This explains the small differences between FastIsostasy and Seakon in the coupled runs, supporting the use of FastIsostasy rather than ELRA in ice sheet models. The computation time of FastIsostasy ranged between 1 and 5 minutes on a single GPU, for the strong and weak Earth model, respectively. In stark contrast, computation time of Seakon was ca. 2.5 days on 288 CPU cores. Thus, FastIsostasy is as efficient as ELRA models and is additionally well-suited for high resolution simulations of AIS evolution.

https://doi.org/10.5194/egusphere-2026-2640
Preprint. Discussion started: 11 June 2026

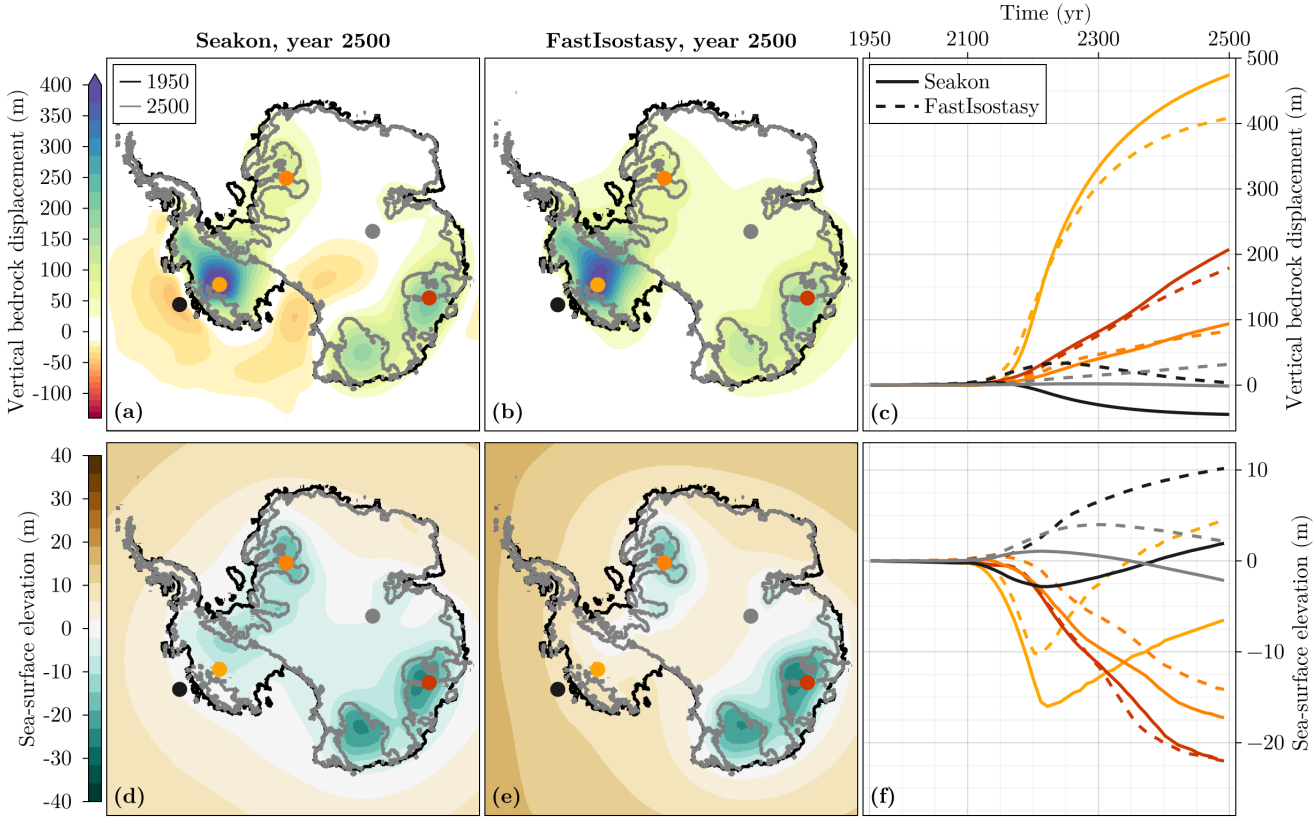

Figure 6. Comparison of GIA predictions using the weak Earth model. Same as Figure 4 but for the Seakon and FastIsostasy coupled simulations with the weak Earth model.

4 Discussion

To understand how adopting FastIsostasy produced more realistic RSL predictions than ELRA models, we compute the contribution to the absolute change in RSL, ΔS_i, of the viscous, elastic, gravitational, and barystatic response, respectively. This is computed as a spatial mean over a mask $\mathcal{M}$, which yields 1 for points that lose ice coverage over the simulation and 0 otherwise. This can be expressed as:

$$\Delta S_i(t) = \text{mean}_{\mathcal{M}}\,\text{abs}(S_i(x,y,t)), \quad \text{with}: \tag{9}$$

$$i \in \{\text{visc}, \text{elas}, \text{grav}, \text{bsl}\}, \tag{10}$$

$$\mathcal{M} = \{(x,y)\,|\,H(x,y,t=1950) > 0 \wedge H(x,y,t=2500) = 0\} \tag{11}$$

https://doi.org/10.5194/egusphere-2026-2640
Preprint. Discussion started: 11 June 2026

Furthermore, we also compute the relative change in RSL, which is computed by dividing each absolute contribution (i.e., viscous, elastic, gravitational, and barystatic contributions) by the sum of all four absolute contributions. The resulting decomposition displays a clear time dependence (Fig. 7), and the relative importance of the viscous contribution increases over time.

For the weak Earth model, the relative contribution of the viscous response has a magnitude comparable to the sum of the others at year 2020 and lasting until 2500. In contrast, for the strong Earth model, the instantaneous responses are comparatively larger, on average, than the viscous response over the whole 1950-2500 period (Fig. 7). This highlights the importance of representing the instantaneous responses, especially when the prediction horizon is relatively short and/or the upper mantle viscosity is relatively high. Contrary to ELRA models, FastIsostasy approximates both the gravitational and elastic responses, which partly explains its reduced error metrics compared to the ELRA models. We emphasise that including these responses in ELRA is straightforward but seldom applied.

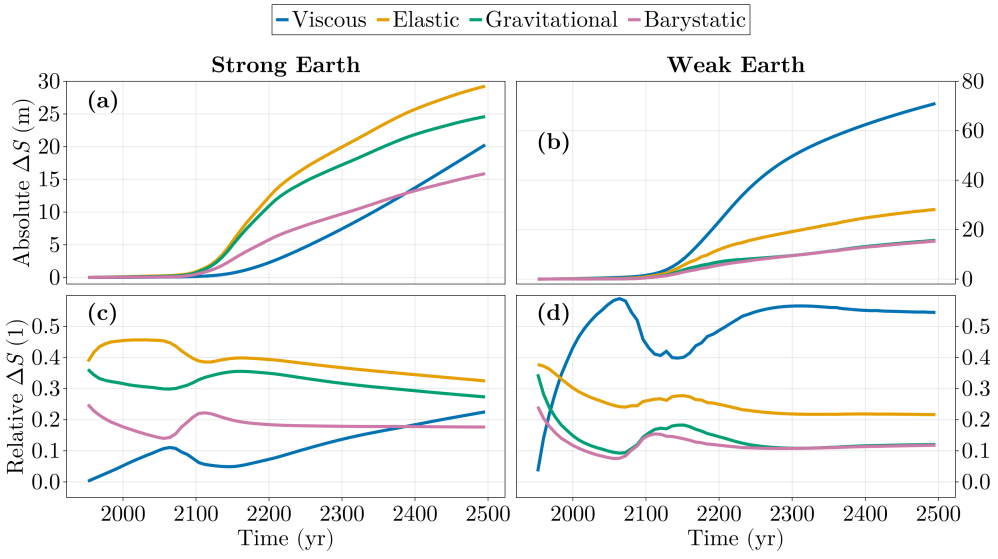

Figure 7. Decomposition of the viscous, elastic, gravitational, and barystatic contributions to RSL in the FastIsostasy coupled simulations. Decomposition of the (a-b) absolute and (c-d) relative contributions to RSL of the viscous, elastic, gravitational and barystatic response for the strong and weak Earth model.

Moreover, GIA models that assume a viscous asthenosphere, such as FastIsostasy, offer important advantages over models that assume a relaxed asthenosphere, such as ELRA models. Although the viscosity variations have to be "lumped" from 3-D to 2-D for use in FastIsostasy, no empirically-derived relation between relaxation time and upper mantle viscosity is needed. Furthermore, the timescale of viscous asthenosphere adjustment depends on the spatial extent of the surface load anomaly, which is also the case in 3-D GIA models, but not the case in ELRA models. This is another reason for the low error metrics of FastIsostasy and is further bolstered by the inclusion of a laterally-variable lithosphere. In contrast, ELRA models typically assume a constant lithospheric thickness (Le Meur and Huybrechts, 1996; van Calcar et al., 2026). A modified formulation of

https://doi.org/10.5194/egusphere-2026-2640
Preprint. Discussion started: 11 June 2026

ELRA allows lateral variations in lithospheric thickness, however, at much higher computational cost than FastIsostasy due to the linear system of equations that needs to be solved at each time step (Coulon et al., 2021).

To address some of the limitations of the ELRA model, Adhikari et al. (2025) suggested a set of Green's functions that can be convolved with the load to obtain the elastic, viscous and gravitational response. While this is a useful approach for approximating the behaviour of a 1-D GIA model at low computational cost, it is incapable of representing the 3-D structure of the Earth and, therefore, has limited applicability in Antarctic-wide studies. With a similar motivation, van Calcar et al. (2026) also recently proposed a 1-D structure of the solid-Earth that reduces the error of AIS contribution to sea level rise compared to simulations using a 3-D GIA model. However, the 1-D GIA model in van Calcar et al. (2026) adopts an upper mantle viscosity of $10^{19}\mathrm{Pas}$, which is unrealistically low at the continental-scale and beyond. There are several major issues that ice sheet modellers will face if they chose to adopt a 1-D global GIA model that solves the sea level equation, as in the approach of van Calcar et al. (2026). First, the implementation/coupling effort and computational cost of a 1-D global GIA model is generally too high for ice sheet modellers. Second, laterally-constant Earth structure is not well-suited for AIS projections if retreat occurs in both West and East Antarctica, as these two regions have fundamentally different solid Earth structure that cannot be represented with a single parameter.

To approximate ice sheet evolution in simulations coupled with 3-D GIA models, van Calcar et al. (2026) also proposed that different relaxation times could be used in ELRA models in simulations over different time horizons (e.g., 300 years versus 500 years). However, the present work makes it clear that the validity of using a laterally-uniform Earth structure not only depends on the prediction time horizon but also on the location of ice retreat and upper mantle viscosity in regions undergoing retreat. The limitation of laterally-uniform models is well-illustrated by our comparisons with the ELRA500 and ELRA3000 simulations which, besides leading to biased sea level contributions, also produce significant differences in the projected ice thickness changes relative to the Seakon simulations with 3-D Earth structure (Figs. 4, S4-S10). Accurately capturing ice thickness changes is critical when the triggering of ice sheet non-linearities depends on the location of the grounding line, as is the case for the marine ice sheet instability, which is likely to be the main mechanism driving future abrupt sea level rise (Seroussi et al., 2024).

As highlighted by Figs. 5 & 6, the parametric uncertainties of the solid Earth are more important than the model uncertainties for projections of the GIA response to AIS retreat. Therefore, improved uncertainty quantification in future AIS contributions to sea level rise requires a broader range of Earth structure realizations. Despite uncertainty and ongoing debate associated with the rheological model that is best suited to represent solid Earth deformation in Antarctica (e.g. Blank et al., 2021; Lau et al., 2021), the strong and weak Earth models adopted here represent near end-member models of Antarctic-wide Earth structure in the literature that may be useful for upcoming multi-century ice sheet projection efforts, such as ISMIP7.

Although FastIsostasy was originally developed to solve the laterally variable ELVA equations with explicit time stepping (Swierczek-Jereczek et al., 2024), other models of viscous deformation have been included in FastIsostasy since then (ELRA, optionally with 2-D relaxation timescale; ELVA with implicit time stepping as proposed by Bueler et al. (2007); and soon the approach of Adhikari et al. (2025)). FastIsostasy can therefore be increasingly understood as a collection of fast GIA models for ice sheet modelling.

https://doi.org/10.5194/egusphere-2026-2640
Preprint. Discussion started: 11 June 2026

The present work does not use the newest datasets for subglacial topography (e.g., Pritchard et al., 2025) or climate forcings (e.g. those used in Coulon et al., 2025). However, we again stress that the aim of this work is not to provide estimates of future sea level rise but rather to demonstrate that FastIsostasy can accurately approximate the 3-D GIA response, even under extreme ice loss scenarios such as RCP8.5-MICI.

5 Conclusions

We evaluate the performance of the FastIsostasy GIA model (Swierczek-Jereczek et al., 2024) versus the Seakon 3-D GIA model (Latychev et al., 2005) in iteratively coupled ice sheet - GIA simulations of AIS evolution over the next five centuries. Unlike the ELRA approach and the approaches recently proposed by van Calcar et al. (2026) and Adhikari et al. (2025), FastIsostasy can account for realistic lateral variations in solid Earth structure across Antarctica and approximate both the deformational and gravitational response to changes in surface loading. Coupled simulations employing FastIsostasy yield predictions of ice thickness, grounding line evolution, vertical bed displacement, and sea surface elevation that are comparable to those obtained using the substantially more computationally-expensive Seakon 3-D GIA model. Coupled simulations adopting the strong and weak Earth models - which span a broad range of viscoelastic Earth structures recently inferred for Antarctica - demonstrate the robust performance of FastIsostasy relative to Seakon, regardless of the assumed Earth structure. Compared to other computationally efficient GIA models, FastIsostasy significantly improves the representation of bedrock deformation and sea level change, while taking into account laterally-variable Earth structure. Thus, FastIsostasy offers an open-source, computationally efficient, and accurate approach for ice sheet modellers who want to reduce biases in AIS contribution to multi-century projections of sea level rise.

Code and data availability. The source code of FastIsostasy can be found at https://github.com/palma-ice/yelmo and https://github.com/JanJereczek/FastIsostasy.jl. The code used to generate the figures can be found at https://github.com/JanJereczek/fastiso-ssp2500. A reduced dataset of the simulation results will be archived upon publication. Due to the sheer size of the full dataset, specific outputs can be shared upon request.

Appendix A: Lumping of the 3-D viscosity

To obtain the low errors presented here, we performed minimal tuning of FastIsostasy to investigate the optimal approach to derive the 2-D effective viscosity from a 3-D field, a task referred to as viscosity lumping. The induction proposed by Swierczek-Jereczek et al. (2024) only holds for homogeneous viscosities, leaving the following question open: what lumping method minimises the error of FastIsostasy compared to a 3-D GIA model? We investigated several approaches for mapping the 3-D viscosity field into a 2-D one:

1. Use the viscosity at a reference depth z_1. For the present analysis, we set $z_0 = 400\,\mathrm{km}$.

https://doi.org/10.5194/egusphere-2026-2640
Preprint. Discussion started: 11 June 2026

2. Average the viscosity over a reference depth $z_1 < z < z_2$. For the present analysis, we set $z_1 = 200\,\mathrm{km}$ and $z_2 = 500\,\mathrm{km}$.

3. Use the viscosity at a reference depth below the lithosphere $z_0 = T(x,y) + \Delta z$). For the present analysis, we set $\Delta z = 150\,\mathrm{km}$.

4. Average the viscosity over a reference depth below the lithosphere $T(x,y) < z < T(x,y) + \Delta z$. Here again we set $\Delta z = 150\,\mathrm{km}$.

5. Use the minimum viscosity over a reference depth below the lithosphere $T(x,y) < z < T(x,y) + \Delta z$. Here again we set $\Delta z = 150\,\mathrm{km}$.

These approaches are referred to as *absolute depth, absolute average, relative depth, relative average* and *min* in Figs. A1-A2. We perform a FastIsostasy run from 1950 to 2500 under RCP8.5 for each of these lumping method, both for the weak and the strong solid-Earth models. We compute the maximal and mean absolute errors in RSL s as:

$$e_{\max}(t=\tilde{t}) = \max_{\mathcal{M}} \mathrm{abs}\left(s_{\mathrm{seakon}}(x,y,\tilde{t}) - s_{\mathrm{fastiso}}(x,y,\tilde{t})\right) \quad \text{(A1)}$$

$$e_{\mathrm{mean}}(t=\tilde{t}) = \mathrm{mean}_{\mathcal{M}} \mathrm{abs}\left(s_{\mathrm{seakon}}(x,y,\tilde{t}) - s_{\mathrm{fastiso}}(x,y,\tilde{t})\right) \quad \text{(A2)}$$

Here again, $\mathcal{M} = \{(x,y) \,|\, H(x,y,t=1950) > 0 \wedge H(x,y,t=2500) = 0\}$ denotes the mask of points that became ice-free during the simulation. The results show that the method using the minimum viscosity over a reference depth below the lithosphere yields the best results, both for the strong and weak Earth models (Fig. A1 and Fig. A2, respectively). More specifically, this yields the lowest maximal error of all lumping methods, and we therefore use this approach for all the results shown in the remainder of the paper. In contrast, the other methods tend to underestimate the maximal RSL change in the case of a weak Earth. However, the relative depth and absolute mean approaches also yield error metrics that can be considered sufficiently good for many applications. It appears that only the relative mean and absolute depth approaches systematically yield some of the largest error metrics.

We stress that the numerical values used in (LV-)ELRA have been obtained by tuning on examples that differ from our current setup (van Calcar et al., 2026). To prevent an unfair comparison, the numerical values associated with each lumping method for FastIsostasy have not been tuned and stem only from a guess informed by physical understanding of the process. Thus, improved performance may be achieved with additional effort.

Competing interests. The authors declare no competing interests.

Author contributions. J.S-J. performed the FastIsostasy and LV-ELRA runs, E.M.L. performed the Seakon and PSUICE3D runs. Both authors drafted the manuscript and the figures with contributions from all co-authors.

Funding. J.S.-J. received funding from the EU H2020 research infrastructures of the European Commission (ClimTip, grant no. 101137601). This research was supported by the Natural Sciences and Engineering Research Council of Canada (grant no.

https://doi.org/10.5194/egusphere-2026-2640
Preprint. Discussion started: 11 June 2026

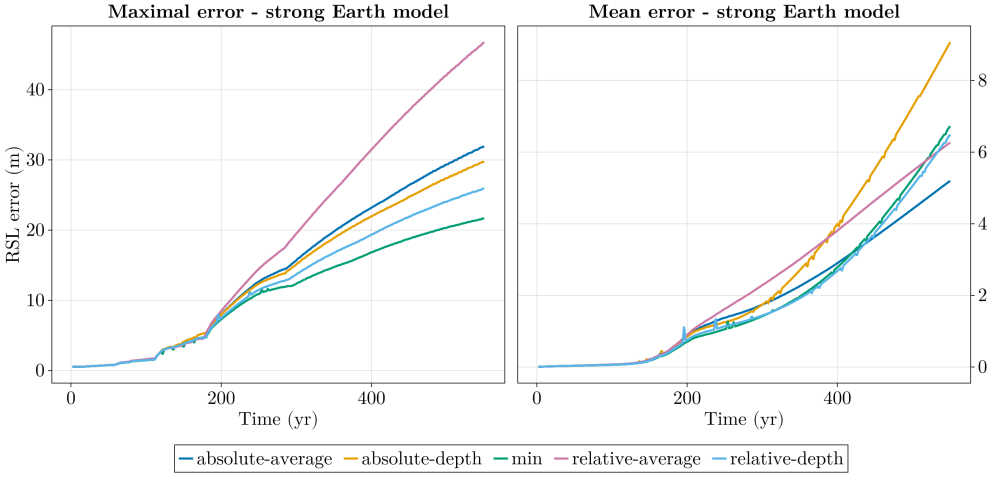

Figure A1. Maximal and mean errors of the lumping methods for the strong Earth model.

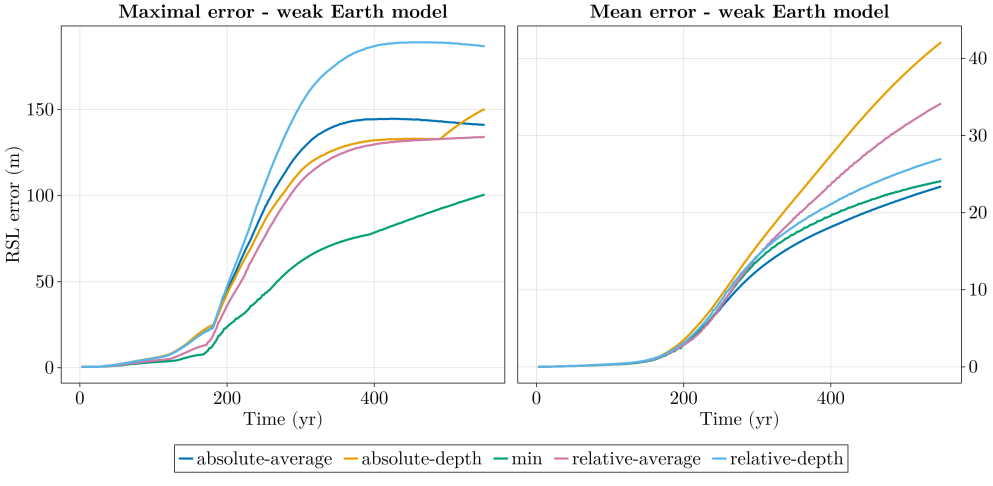

Figure A2. Maximal and mean errors of the lumping methods for the weak Earth model.

https://doi.org/10.5194/egusphere-2026-2640
Preprint. Discussion started: 11 June 2026

RGPIN-2016-05159 to NG). A.J.L. acknowledges support from the Vetlesen Foundation and NSF OPP-2142592.

Acknowledgments. We acknowledge the ISMIP7 community and, specifically, the GIA and Sea Level Focus Group for inspiring this study. We also acknowledge the NSF-funded POLENET-ANET project.

https://doi.org/10.5194/egusphere-2026-2640
Preprint. Discussion started: 11 June 2026

References

Adhikari, S., Caron, L., Han, H. K., Houriez, L., Larour, E., and Ivins, E.: Enabling ice sheet models to capture solid Earth feedback with ease and accuracy, https://doi.org/10.5194/egusphere-2025-3561, 2025.

An, M., Wiens, D. A., Zhao, Y., Feng, M., Nyblade, A., Kanao, M., Li, Y., Maggi, A., and Lévêque, J.-J.: Temperature, lithosphere-asthenosphere boundary, and heat flux beneath the Antarctic Plate inferred from seismic velocities, Journal of Geophysical Research: Solid Earth, 120, 8720–8742, https://doi.org/10.1002/2015JB011917, _eprint: https://agupubs.onlinelibrary.wiley.com/doi/pdf/10.1002/2015JB011917, 2015.

Austermann, J., Mitrovica, J. X., Latychev, K., and Milne, G. A.: Barbados-based estimate of ice volume at Last Glacial Maximum affected by subducted plate, Nature Geoscience, 6, 553–557, https://doi.org/10.1038/ngeo1859, 2013.

Austermann, J., Hoggard, M. J., Latychev, K., Richards, F. D., and Mitrovica, J. X.: The effect of lateral variations in Earth structure on Last Interglacial sea level, Geophysical Journal International, 227, 1938–1960, https://doi.org/10.1093/gji/ggab289, 2021.

Barletta, V. R., Bevis, M., Smith, B. E., Wilson, T., Brown, A., Bordoni, A., Willis, M., Khan, S. A., Rovira-Navarro, M., Dalziel, I., Smalley, R., Kendrick, E., Konfal, S., Caccamise, D. J., Aster, R. C., Nyblade, A., and Wiens, D. A.: Observed rapid bedrock uplift in Amundsen Sea Embayment promotes ice-sheet stability, Science, 360, 1335–1339, https://doi.org/10.1126/science.aao1447, 2018.

Blank, B., Barletta, V., Hu, H., Pappa, F., and van der Wal, W.: Effect of Lateral and Stress-Dependent Viscosity Variations on GIA Induced Uplift Rates in the Amundsen Sea Embayment, Geochemistry, Geophysics, Geosystems, 22, e2021GC009 807, https://doi.org/10.1029/2021GC009807, _eprint: https://agupubs.onlinelibrary.wiley.com/doi/pdf/10.1029/2021GC009807, 2021.

Brown, S. E. and Fischer, K. M.: Investigating the Antarctic Lithosphere Through Sp Receiver Function Analysis, Geochemistry, Geophysics, Geosystems, 26, e2025GC012 268, https://doi.org/10.1029/2025GC012268, _eprint: https://agupubs.onlinelibrary.wiley.com/doi/pdf/10.1029/2025GC012268, 2025.

Bueler, E., Lingle, C. S., and Brown, J.: Fast computation of a viscoelastic deformable Earth model for ice-sheet simulations, Annals of Glaciology, 46, 97–105, https://doi.org/10.3189/172756407782871567, 2007.

Cathles, L. M.: Viscosity of the Earth's Mantle, Princeton University Press, 1975.

Chua, E. L. and Lebedev, S.: Waveform tomography of the Antarctic Plate, Geophysical Journal International, 241, 219–240, https://doi.org/10.1093/gji/ggaf041, 2025.

Coulon, V., Bulthuis, K., Whitehouse, P. L., Sun, S., Haubner, K., Zipf, L., and Pattyn, F.: Contrasting Response of West and East Antarctic Ice Sheets to Glacial Isostatic Adjustment, Journal of Geophysical Research: Earth Surface, 126, https://doi.org/10.1029/2020JF006003, 2021.

Coulon, V., Klose, A. K., Edwards, T., Turner, F., Pattyn, F., and Winkelmann, R.: From short-term uncertainties to long-term certainties in the future evolution of the Antarctic Ice Sheet, Nature Communications, 16, 10 385, https://doi.org/10.1038/s41467-025-66178-w, 2025.

DeConto, R. M. and Pollard, D.: Contribution of Antarctica to past and future sea-level rise, Nature, 531, 591–597, https://doi.org/10.1038/nature17145, 2016.

DeConto, R. M., Pollard, D., Alley, R. B., Velicogna, I., Gasson, E., Gomez, N., Sadai, S., Condron, A., Gilford, D. M., Ashe, E. L., Kopp, R. E., Li, D., and Dutton, A.: The Paris Climate Agreement and future sea-level rise from Antarctica, Nature, 593, 83–89, https://doi.org/10.1038/s41586-021-03427-0, 2021.

Fox-Kemperer, B., Hewitt, H. T., and Xiao, C.: Ocean, Cryosphere, and Sea Level Change, Cambridge University Press, 1 edn., ISBN 978-1-009-15789-6, https://doi.org/10.1017/9781009157896, 2021.

https://doi.org/10.5194/egusphere-2026-2640
Preprint. Discussion started: 11 June 2026

Fretwell, P., Pritchard, H. D., Vaughan, D. G., Bamber, J. L., Barrand, N. E., Bell, R., Bianchi, C., Bingham, R. G., Blankenship, D. D., Casassa, G., Catania, G., Callens, D., Conway, H., Cook, A. J., Corr, H. F. J., Damaske, D., Damm, V., Ferraccioli, F., Forsberg, R., Fujita, S., Gim, Y., Gogineni, P., Griggs, J. A., Hindmarsh, R. C. A., Holmlund, P., Holt, J. W., Jacobel, R. W., Jenkins, A., Jokat, W., Jordan, T., King, E. C., Kohler, J., Krabill, W., Riger-Kusk, M., Langley, K. A., Leitchenkov, G., Leuschen, C., Luyendyk, B. P., Matsuoka, K., Mouginot, J., Nitsche, F. O., Nogi, Y., Nost, O. A., Popov, S. V., Rignot, E., Rippin, D. M., Rivera, A., Roberts, J., Ross, N., Siegert, M. J., Smith, A. M., Steinhage, D., Studinger, M., Sun, B., Tinto, B. K., Welch, B. C., Wilson, D., Young, D. A., Xiangbin, C., and Zirizzotti, A.: Bedmap2: improved ice bed, surface and thickness datasets for Antarctica, The Cryosphere, 7, 375–393, https://doi.org/10.5194/tc-7-375-2013, 2013.

Goelzer, H., Coulon, V., Pattyn, F., de Boer, B., and van de Wal, R.: Brief communication: On calculating the sea-level contribution in marine ice-sheet models, The Cryosphere, 14, 833–840, https://doi.org/10.5194/tc-14-833-2020, 2020.

Gomez, N., Mitrovica, J. X., Huybers, P., and Clark, P. U.: Sea level as a stabilizing factor for marine-ice-sheet grounding lines, Nature Geoscience, 3, 850–853, https://doi.org/10.1038/ngeo1012, 2010.

Gomez, N., Pollard, D., Mitrovica, J. X., Huybers, P., and Clark, P. U.: Evolution of a coupled marine ice sheet-sea level model, Journal of Geophysical Research: Earth Surface, 117, https://doi.org/10.1029/2011JF002128, 2012.

Gomez, N., Pollard, D., and Mitrovica, J. X.: A 3-D coupled ice sheet – sea level model applied to Antarctica through the last 40 ky, Earth and Planetary Science Letters, 384, 88–99, https://doi.org/10.1016/j.epsl.2013.09.042, 2013.

Gomez, N., Pollard, D., and Holland, D.: Sea-level feedback lowers projections of future Antarctic Ice-Sheet mass loss, Nature Communications, 6, 8798, https://doi.org/10.1038/ncomms9798, 2015.

Gomez, N., Latychev, K., and Pollard, D.: A Coupled Ice Sheet–Sea Level Model Incorporating 3D Earth Structure: Variations in Antarctica during the Last Deglacial Retreat, Journal of Climate, 31, 4041–4054, https://doi.org/10.1175/JCLI-D-17-0352.1, 2018.

Gomez, N., Yousefi, M., Pollard, D., DeConto, R. M., Sadai, S., Lloyd, A., Nyblade, A., Wiens, D. A., Aster, R. C., and Wilson, T.: The influence of realistic 3D mantle viscosity on Antarctica's contribution to future global sea levels, Science Advances, 10, eadn1470, https://doi.org/10.1126/sciadv.adn1470, 2024.

Hansen, S. E. and Emry, E. L.: East Antarctic tectonic basin structure and its implications for ice-sheet modeling and sea-level projections, Communications Earth & Environment, 6, 138, https://doi.org/10.1038/s43247-025-02140-4, 2025.

Hazzard, J. A. N., Richards, F. D., Goes, S. D. B., and Roberts, G. G.: Probabilistic Assessment of Antarctic Thermomechanical Structure: Impacts on Ice Sheet Stability, Journal of Geophysical Research: Solid Earth, 128, e2023JB026653, https://doi.org/10.1029/2023JB026653, _eprint: https://agupubs.onlinelibrary.wiley.com/doi/pdf/10.1029/2023JB026653, 2023.

Ivins, E. R., van der Wal, W., Wiens, D. A., Lloyd, A. J., and Caron, L.: Antarctic upper mantle rheology, Geological Society, London, Memoirs, 56, M56–2020–19, https://doi.org/10.1144/M56-2020-19, 2022.

Kaufmann, G., Wu, P., and Ivins, E. R.: Lateral viscosity variations beneath Antarctica and their implications on regional rebound motions and seismotectonics, Journal of Geodynamics, 39, 165–181, https://doi.org/10.1016/j.jog.2004.08.009, 2005.

Kendall, R. A., Mitrovica, J. X., and Milne, G. A.: On post-glacial sea level - II. Numerical formulation and comparative results on spherically symmetric models, Geophysical Journal International, 161, 679–706, https://doi.org/10.1111/j.1365-246X.2005.02553.x, 2005.

Konrad, H., Sasgen, I., Pollard, D., and Klemann, V.: Potential of the solid-Earth response for limiting long-term West Antarctic Ice Sheet retreat in a warming climate, Earth and Planetary Science Letters, 432, 254–264, https://doi.org/10.1016/j.epsl.2015.10.008, 2015.

https://doi.org/10.5194/egusphere-2026-2640
Preprint. Discussion started: 11 June 2026

Kustowski, B., Ekström, G., and Dziewoński, A. M.: Anisotropic shear-wave velocity structure of the Earth's mantle: A global model, Journal of Geophysical Research: Solid Earth, 113, https://doi.org/10.1029/2007JB005169, _eprint: https://agupubs.onlinelibrary.wiley.com/doi/pdf/10.1029/2007JB005169, 2008.

Larour, E., Seroussi, H., Adhikari, S., Ivins, E., Caron, L., Morlighem, M., and Schlegel, N.: Slowdown in Antarctic mass loss from solid Earth and sea-level feedbacks, Science, 364, eaav7908, https://doi.org/10.1126/science.aav7908, 2019.

Latychev, K., Mitrovica, J. X., Tromp, J., Tamisiea, M. E., Komatitsch, D., and Christara, C. C.: Glacial isostatic adjustment on 3-D Earth models: a finite-volume formulation, Geophysical Journal International, 161, 421–444, https://doi.org/10.1111/j.1365-246X.2005.02536.x, 2005.

Lau, H. C. P., Austermann, J., Holtzman, B. K., Havlin, C., Lloyd, A. J., Book, C., and Hopper, E.: Frequency Dependent Mantle Viscoelasticity via the Complex Viscosity: Cases From Antarctica, Journal of Geophysical Research: Solid Earth, 126, e2021JB022 622, https://doi.org/10.1029/2021JB022622, _eprint: https://agupubs.onlinelibrary.wiley.com/doi/pdf/10.1029/2021JB022622, 2021.

Le Meur, E. and Huybrechts, P.: A comparison of different ways of dealing with isostasy: examples from modelling the Antarctic ice sheet during the last glacial cycle, Annals of Glaciology, 23, 309–317, https://doi.org/10.3189/S0260305500013586, 1996.

Lei, W., Ruan, Y., Bozdağ, E., Peter, D., Lefebvre, M., Komatitsch, D., Tromp, J., Hill, J., Podhorszki, N., and Pugmire, D.: Global adjoint tomography—model GLAD-M25, Geophysical Journal International, 223, 1–21, https://doi.org/10.1093/gji/ggaa253, 2020.

Lingle, C. S. and Clark, J. A.: A numerical model of interactions between a marine ice sheet and the solid earth: Application to a West Antarctic ice stream, Journal of Geophysical Research, 90, 1100, https://doi.org/10.1029/JC090iC01p01100, 1985.

Lipscomb, W. H., Price, S. F., Hoffman, M. J., Leguy, G. R., Bennett, A. R., Bradley, S. L., Evans, K. J., Fyke, J. G., Kennedy, J. H., Perego, M., Ranken, D. M., Sacks, W. J., Salinger, A. G., Vargo, L. J., and Worley, P. H.: Description and evaluation of the Community Ice Sheet Model (CISM) v2.1, Geoscientific Model Development, 12, 387–424, https://doi.org/10.5194/gmd-12-387-2019, 2019.

Lloyd, A. J., Wiens, D. A., Zhu, H., Tromp, J., Nyblade, A. A., Aster, R. C., Hansen, S. E., Dalziel, I. W. D., Wilson, T., Ivins, E. R., and O'Donnell, J. P.: Seismic Structure of the Antarctic Upper Mantle Imaged with Adjoint Tomography, Journal of Geophysical Research: Solid Earth, 125, 2019JB017 823, https://doi.org/10.1029/2019JB017823, 2020.

Lloyd, A. J., Crawford, O., Al-Attar, D., Austermann, J., Hoggard, M. J., Richards, F. D., and Syvret, F.: GIA imaging of 3-D mantle viscosity based on palaeo sea level observations – Part I: Sensitivity kernels for an Earth with laterally varying viscosity, Geophysical Journal International, 236, 1139–1171, https://doi.org/10.1093/gji/ggad455, 2024.

Lucas, E. M., Soto, D., Nyblade, A. A., Lloyd, A. J., Aster, R. C., Wiens, D. A., O'Donnell, J. P., Stuart, G. W., Wilson, T. J., Dalziel, I. W., Winberry, J. P., and Huerta, A. D.: P- and S-wave velocity structure of central West Antarctica: Implications for the tectonic evolution of the West Antarctic Rift System, Earth and Planetary Science Letters, 546, 116 437, https://doi.org/10.1016/j.epsl.2020.116437, 2020.

Lucas, E. M., Nyblade, A. A., Lloyd, A. J., Aster, R. C., Wiens, D. A., O'Donnell, J. P., Stuart, G. W., Wilson, T. J., Dalziel, I. W. D., Winberry, J. P., and Huerta, A. D.: Seismicity and Pn Velocity Structure of Central West Antarctica, Geochemistry, Geophysics, Geosystems, 22, e2020GC009 471, https://doi.org/10.1029/2020GC009471, _eprint: https://agupubs.onlinelibrary.wiley.com/doi/pdf/10.1029/2020GC009471, 2021.

Lucas, E. M., Gomez, N., and Wilson, T.: The impact of regional-scale upper-mantle heterogeneity on glacial isostatic adjustment in West Antarctica, The Cryosphere, 19, 2387–2405, https://doi.org/10.5194/tc-19-2387-2025, 2025.

Meinshausen, M., Smith, S. J., Calvin, K., Daniel, J. S., Kainuma, M. L. T., Lamarque, J.-F., Matsumoto, K., Montzka, S. A., Raper, S. C. B., Riahi, K., Thomson, A., Velders, G. J. M., and Van Vuuren, D. P.: The RCP greenhouse gas concentrations and their extensions from 1765 to 2300, Climatic Change, 109, 213–241, https://doi.org/10.1007/s10584-011-0156-z, 2011.

https://doi.org/10.5194/egusphere-2026-2640
Preprint. Discussion started: 11 June 2026

Milne, G. A. and Mitrovica, J. X.: Postglacial sea-level change on a rotating Earth, Geophysical Journal International, 133, 1–19, https://doi.org/10.1046/j.1365-246X.1998.1331455.x, 1998.

Mitrovica, J. X. and Milne, G. A.: On post-glacial sea level: I. General theory, Geophysical Journal International, 154, 253–267, https://doi.org/10.1046/j.1365-246X.2003.01942.x, 2003.

Mitrovica, J. X., Wahr, J., Matsuyama, I., and Paulson, A.: The rotational stability of an ice-age earth, Geophysical Journal International, 161, 491–506, https://doi.org/10.1111/j.1365-246X.2005.02609.x, 2005.

Nield, G. A., Barletta, V. R., Bordoni, A., King, M. A., Whitehouse, P. L., Clarke, P. J., Domack, E., Scambos, T. A., and Berthier, E.: Rapid bedrock uplift in the Antarctic Peninsula explained by viscoelastic response to recent ice unloading, Earth and Planetary Science Letters, 397, 32–41, https://doi.org/10.1016/j.epsl.2014.04.019, 2014.

Nield, G. A., Whitehouse, P. L., King, M. A., and Clarke, P. J.: Glacial isostatic adjustment in response to changing Late Holocene behaviour of ice streams on the Siple Coast, West Antarctica, Geophysical Journal International, 205, 1–21, https://doi.org/10.1093/gji/ggv532, 2016.

Nield, G. A., Whitehouse, P. L., van der Wal, W., Blank, B., O'Donnell, J. P., and Stuart, G. W.: The impact of lateral variations in lithospheric thickness on glacial isostatic adjustment in West Antarctica, Geophysical Journal International, 214, 811–824, https://doi.org/10.1093/gji/ggy158, 2018.

Nield, G. A., King, M. A., Koulali, A., and Samrat, N.: Postseismic Deformation in the Northern Antarctic Peninsula Following the 2003 and 2013 Scotia Sea Earthquakes, Journal of Geophysical Research: Solid Earth, 128, e2023JB026 685, https://doi.org/10.1029/2023JB026685, _eprint: https://agupubs.onlinelibrary.wiley.com/doi/pdf/10.1029/2023JB026685, 2023.

Nield, G. A., Bentley, M. J., Koulali, A., Clarke, P. J., King, M. A., Wilson, T., and Whitehouse, P. L.: Surface Mass Balance Variability Causes Viscoelastic Solid Earth Deformation in the Antarctic Peninsula, Geophysical Research Letters, 52, e2025GL114 595, https://doi.org/10.1029/2025GL114595, _eprint: https://agupubs.onlinelibrary.wiley.com/doi/pdf/10.1029/2025GL114595, 2025.

NOAA National Centers for Environmental Information: ETOPO 2022 15 Arc-Second Global Relief Model, NOAA National Centers for Environmental Information, https://doi.org/10.25921/fd45-gt74, accessed: 2026-06-09, 2022.

Nowicki, S. M. J., Payne, A., Larour, E., Seroussi, H., Goelzer, H., Lipscomb, W., Gregory, J., Abe-Ouchi, A., and Shepherd, A.: Ice Sheet Model Intercomparison Project (ISMIP6) contribution to CMIP6, Geoscientific Model Development, 9, 4521–4545, https://doi.org/10.5194/gmd-9-4521-2016, num Pages: 4521-4545, 2016.

Pattyn, F.: Sea-level response to melting of Antarctic ice shelves on multi-centennial timescales with the fast Elementary Thermomechanical Ice Sheet model (f.ETISh v1.0), The Cryosphere, 11, 1851–1878, https://doi.org/10.5194/tc-11-1851-2017, 2017.

Peltier, W. R., Argus, D. F., and Drummond, R.: Comment on "An Assessment of the ICE-6G_C (VM5a) Glacial Isostatic Adjustment Model" by Purcell et al., Journal of Geophysical Research: Solid Earth, 123, 2019–2028, https://doi.org/10.1002/2016JB013844, 2018.

Pollard, D. and DeConto, R. M.: Description of a hybrid ice sheet-shelf model, and application to Antarctica, Geoscientific Model Development, 5, 1273–1295, https://doi.org/10.5194/gmd-5-1273-2012, 2012.

Pollard, D. and DeConto, R. M.: Continuous simulations over the last 40 million years with a coupled Antarctic ice sheet-sediment model, Palaeogeography, Palaeoclimatology, Palaeoecology, 537, 109 374, https://doi.org/10.1016/j.palaeo.2019.109374, 2020.

Pollard, D., DeConto, R. M., and Alley, R. B.: Potential Antarctic Ice Sheet retreat driven by hydrofracturing and ice cliff failure, Earth and Planetary Science Letters, 412, 112–121, https://doi.org/10.1016/j.epsl.2014.12.035, 2015.

Powell, E., Gomez, N., Hay, C., Latychev, K., and Mitrovica, J. X.: Viscous Effects in the Solid Earth Response to Modern Antarctic Ice Mass Flux: Implications for Geodetic Studies of WAIS Stability in a Warming World, Journal of Climate, 33, 443–459, https://doi.org/10.1175/JCLI-D-19-0479.1, 2020.

https://doi.org/10.5194/egusphere-2026-2640
Preprint. Discussion started: 11 June 2026

Pritchard, H. D., Fretwell, P. T., Fremand, A. C., Bodart, J. A., Kirkham, J. D., Aitken, A., Bamber, J., Bell, R., Bianchi, C., Bingham, R. G., Blankenship, D. D., Casassa, G., Christianson, K., Conway, H., Corr, H. F. J., Cui, X., Damaske, D., Damm, V., Dorschel, B., Drews, R., Eagles, G., Eisen, O., Eisermann, H., Ferraccioli, F., Field, E., Forsberg, R., Franke, S., Goel, V., Gogineni, S. P., Greenbaum, J., Hills, B., Hindmarsh, R. C. A., Hoffman, A. O., Holschuh, N., Holt, J. W., Humbert, A., Jacobel, R. W., Jansen, D., Jenkins, A., Jokat, W., Jong, L., Jordan, T. A., King, E. C., Kohler, J., Krabill, W., Maton, J., Gillespie, M. K., Langley, K., Lee, J., Leitchenkov, G., Leuschen, C., Luyendyk, B., MacGregor, J. A., MacKie, E., Moholdt, G., Matsuoka, K., Morlighem, M., Mouginot, J., Nitsche, F. O., Nost, O. A., Paden, J., Pattyn, F., Popov, S., Rignot, E., Rippin, D. M., Rivera, A., Roberts, J. L., Ross, N., Ruppel, A., Schroeder, D. M., Siegert, M. J., Smith, A. M., Steinhage, D., Studinger, M., Sun, B., Tabacco, I., Tinto, K. J., Urbini, S., Vaughan, D. G., Wilson, D. S., Young, D. A., and Zirizzotti, A.: Bedmap3 updated ice bed, surface and thickness gridded datasets for Antarctica, Scientific Data, 12, 414, https://doi.org/10.1038/s41597-025-04672-y, 2025.

Richards, F. D., Hoggard, M. J., White, N., and Ghelichkhan, S.: Quantifying the Relationship Between Short-Wavelength Dynamic Topography and Thermomechanical Structure of the Upper Mantle Using Calibrated Parameterization of Anelasticity, Journal of Geophysical Research: Solid Earth, 125, e2019JB019 062, https://doi.org/10.1029/2019JB019062, _eprint: https://agupubs.onlinelibrary.wiley.com/doi/pdf/10.1029/2019JB019062, 2020.

Ritzwoller, M. H., Shapiro, N. M., Levshin, A. L., and Leahy, G. M.: Crustal and upper mantle structure beneath Antarctica and surrounding oceans, Journal of Geophysical Research: Solid Earth, 106, 30 645–30 670, https://doi.org/10.1029/2001JB000179, _eprint: https://agupubs.onlinelibrary.wiley.com/doi/pdf/10.1029/2001JB000179, 2001.

Robinson, A., Alvarez-Solas, J., Montoya, M., Goelzer, H., Greve, R., and Ritz, C.: Description and validation of the ice-sheet model Yelmo (version 1.0), Geoscientific Model Development, 13, 2805–2823, https://doi.org/10.5194/gmd-13-2805-2020, 2020.

Rückamp, M., Greve, R., and Humbert, A.: Comparative simulations of the evolution of the Greenland ice sheet under simplified Paris Agreement scenarios with the models SICOPOLIS and ISSM, Polar Science, 21, 14–25, https://doi.org/10.1016/j.polar.2018.12.003, 2019.

Samrat, N. H., King, M. A., Watson, C., Hooper, A., Chen, X., Barletta, V. R., and Bordoni, A.: Reduced ice mass loss and three-dimensional viscoelastic deformation in northern Antarctic Peninsula inferred from GPS, Geophysical Journal International, 222, 1013–1022, https://doi.org/10.1093/gji/ggaa229, 2020.

Samrat, N. H., King, M. A., Watson, C., Hay, A., Barletta, V. R., and Bordoni, A.: Upper Mantle Viscosity Underneath Northern Marguerite Bay, Antarctic Peninsula Constrained by Bedrock Uplift and Ice Mass Variability, Geophysical Research Letters, 48, e2021GL097 065, https://doi.org/10.1029/2021GL097065, _eprint: https://agupubs.onlinelibrary.wiley.com/doi/pdf/10.1029/2021GL097065, 2021.

Seroussi, H., Pelle, T., Lipscomb, W. H., Abe-Ouchi, A., Albrecht, T., Alvarez-Solas, J., Asay-Davis, X., Barre, J., Berends, C. J., Bernales, J., Blasco, J., Caillet, J., Chandler, D. M., Coulon, V., Cullather, R., Dumas, C., Galton-Fenzi, B. K., Garbe, J., Gillet-Chaulet, F., Gladstone, R., Goelzer, H., Golledge, N., Greve, R., Gudmundsson, G. H., Han, H. K., Hillebrand, T. R., Hoffman, M. J., Huybrechts, P., Jourdain, N. C., Klose, A. K., Langebroek, P. M., Leguy, G. R., Lowry, D. P., Mathiot, P., Montoya, M., Morlighem, M., Nowicki, S., Pattyn, F., Payne, A. J., Quiquet, A., Reese, R., Robinson, A., Saraste, L., Simon, E. G., Sun, S., Twarog, J. P., Trusel, L. D., Urruty, B., Van Breedam, J., Van De Wal, R. S. W., Wang, Y., Zhao, C., and Zwinger, T.: Evolution of the Antarctic Ice Sheet Over the Next Three Centuries From an ISMIP6 Model Ensemble, Earth's Future, 12, e2024EF004 561, https://doi.org/10.1029/2024EF004561, 2024.

Shen, W., Wiens, D. A., Anandakrishnan, S., Aster, R. C., Gerstoft, P., Bromirski, P. D., Hansen, S. E., Dalziel, I. W. D., Heeszel, D. S., Huerta, A. D., Nyblade, A. A., Stephen, R., Wilson, T. J., and Winberry, J. P.: The Crust and Upper Mantle Structure of Central and West

https://doi.org/10.5194/egusphere-2026-2640
Preprint. Discussion started: 11 June 2026

Antarctica From Bayesian Inversion of Rayleigh Wave and Receiver Functions, Journal of Geophysical Research: Solid Earth, 123, 7824–7849, https://doi.org/10.1029/2017JB015346, _eprint: https://agupubs.onlinelibrary.wiley.com/doi/pdf/10.1029/2017JB015346, 2018.

Swierczek-Jereczek, J., Montoya, M., Latychev, K., Robinson, A., Alvarez-Solas, J., and Mitrovica, J.: FastIsostasy v1.0 – a regional, accelerated 2D glacial isostatic adjustment (GIA) model accounting for the lateral variability of the solid Earth, Geoscientific Model Development, 17, 5263–5290, https://doi.org/10.5194/gmd-17-5263-2024, 2024.

van Calcar, C. J., Bernales, J., Berends, C. J., van der Wal, W., and van de Wal, R. S. W.: Bedrock uplift reduces Antarctic sea-level contribution over next centuries, Nature Communications, 16, 10 512, https://doi.org/10.1038/s41467-025-66435-y, 2025.

van Calcar, C. J., Whitehouse, P. L., van de Wal, R. S. W., and van der Wal, W.: Approximating 3D bedrock deformation in an Antarctic ice-sheet model for projections, The Cryosphere, 20, 757–775, https://doi.org/10.5194/tc-20-757-2026, 2026.

Wan, J. X. W., Gomez, N., Latychev, K., and Han, H. K.: Resolving glacial isostatic adjustment (GIA) in response to modern and future ice loss at marine grounding lines in West Antarctica, The Cryosphere, 16, 2203–2223, https://doi.org/10.5194/tc-16-2203-2022, 2022.

Wiens, D. A., Shen, W., and Lloyd, A. J.: The seismic structure of the Antarctic upper mantle, Geological Society, London, Memoirs, 56, 195–212, https://doi.org/10.1144/M56-2020-18, 2023.

Zhao, C., King, M. A., Watson, C. S., Barletta, V. R., Bordoni, A., Dell, M., and Whitehouse, P. L.: Rapid ice unloading in the Fleming Glacier region, southern Antarctic Peninsula, and its effect on bedrock uplift rates, Earth and Planetary Science Letters, 473, 164–176, https://doi.org/10.1016/j.epsl.2017.06.002, 2017.

Zwally, H. J., Giovinetto, M. B., Beckley, M. A., and Saba, J. L.: Antarctic and Greenland Drainage Systems, 2012.